Titre: Title:	Improving atmospheric water harvesting in carbon-based sorbents through CO₂ activation
Auteurs: Authors:	David Brassard, Seyedemad Alavitabari, Wendell Raphael, Richard Boudreault, Pierre-Luc Girard-Lauriaut, & Jason Robert Tavares
Date:	2024
Type:	Article de revue / Article
Référence: Citation:	Brassard, D., Alavitabari, S., Raphael, W., Boudreault, R., Girard-Lauriaut, P.-L., & Tavares, J. R. (2024). Improving atmospheric water harvesting in carbon-based sorbents through CO₂ activation. Advanced Sustainable Systems, 8(1), 2300309 (10 pages). https://doi.org/10.1002/adsu.202300309

URL de PolyPublie: PolyPublie URL:	https://publications.polymtl.ca/56758/
Version:	Version officielle de l'éditeur / Published version Révisé par les pairs / Refereed
Conditions d'utilisation: Terms of Use:	Creative Commons Attribution-Utilisation non commerciale-Pas d'oeuvre dérivée 4.0 International / Creative Commons Attribution-NonCommercial-NoDerivatives 4.0 International (CC BY-NC-ND)

Document publié chez l'éditeur officiel
Document issued by the official publisher

Titre de la revue: Journal Title:	Advanced Sustainable Systems (vol. 8, no. 1)
Maison d'édition: Publisher:	Wiley
URL officiel: Official URL:	https://doi.org/10.1002/adsu.202300309
Mention légale: Legal notice:	

Improving Atmospheric Water Harvesting in Carbon-Based Sorbents Through CO$_2$ Activation

David Brassard, Seyedemad Alavitabari, Wendell Raphael, Richard Boudreault, Pierre-Luc Girard-Lauriaut, and Jason R. Tavares*

Atmospheric water harvesting (AWH) can serve as an alternative fresh water source in regions with scarce access to drinking water. While many techniques are geographically or seasonally limited, sorbent-based AWH shows the potential for wider application. Low-cost, carbon-based sorbents named nanoporous sponges (NPS) are recently developed, exhibiting fast and repeatable water uptake of 0.14 g g^{-1} at 90% relative pressure. While useful from a cost and daily water yield point of view, there is room for improvement. This article presents an improved production process combining pyrolysis and activation under CO$_2$ in a single step, yielding improved NPS capable of reproducibly reaching a water uptake of 0.47 g g^{-1} at 95% relative pressure while maintaining fast sorption rates. The NPS show significant endurance and are able to maintain stable performance over numerous humidity cycles. An unexpected time-dependant sorption behavior is also identified for NPS produced with a modified synthesis formulation, due to an increase in sodium carbonate residual content.

1. Introduction

Water scarcity poses a significant risk for the long-term viability of many regions around the world.[1] As an appropriate amount of potable water is a fundamental need for human life, solutions to this rising dilemma are necessary to prevent disastrous

D. Brassard, S. Alavitabari, W. Raphael, J. R. Tavares
CREPEC
Chemical Engineering Department
Polytechnique Montreal
2500 Chemin de Polytechnique, Montréal, QC H3T 1J4, Canada
E-mail: jason.tavares@polymtl.ca
R. Boudreault
Awn Nanotech Inc.
1985 55th Ave, Suite 100, Dorval, QC H9P 1G9, Canada
P.-L. Girard-Lauriaut
Department of Chemical Engineering
McGill University
3610 University, Montréal, QC H3A 0C5, Canada

consequences. Ground water and aquifers, desalination plants, and rainwater storage are the main sources of fresh water employed in various parts of the world. However, for all these methods, a source of liquid water is required (rivers, aquifer, seawater, or precipitations). As these traditional sources are unavailable yearly for some regions or seasonally for others, the collection of water from the atmosphere becomes a necessity in some situations. For instance, fog collection and dew harvesting are two traditional methods of atmospheric water harvesting (AWH). Unfortunately, the orographic conditions required to operate fog collectors are geographically and seasonally limited.[2] They simply cannot be scaled globally. On the other hand, dew water harvesters can be used anywhere, but they need a surface that is cool enough for water to condense and thus offer limited production.[3,4]

Sorbent-based AWH systems are alternatives that are independent from geographic features required by traditional sources. These systems are based on materials that can adsorb moisture under ambient conditions and then desorb it, under specific conditions, with energy requirements approaching that of the enthalpy of water vaporization. Compared to refrigeration-based dehumidifiers operated as water collection systems, sorbent-based system operate on a concentrated stream to reduce the energy requirement from the water collection system.

Capillary condensation theory underpins the adsorption and desorption processes that take place on porous surfaces for the purpose of collecting atmospheric water above the dew point. Adsorption and desorption isotherms are obtained by tracking the water uptake when the sorbent is subjected to different relative pressure (equivalent to relative humidity) conditions. The irreversibility that exists between the adsorption and desorption phases is a phenomenon that has a significant influence on the usage of capillary condensation in water harvesting. The existence of hysteresis between the adsorption and desorption isotherms is evidence of this point. To minimize hysteresis, it is important to strive for pore sizes equal or below the critical size and to perform operations at temperatures higher than the critical level.[5,6] As reference, water at 298 K has a critical pore size of 2.2 nm.[7]

Recently, carbon-based absorbents named nanoporous sponges (NPS) were developed for AWH.[8] This porous carbon

ADVANCED
SCIENCE NEWS

www.advancedsciencenews.com

ADVANCED
SUSTAINABLE
SYSTEMS

www.advsustainsys.com

sorbent is produced through the synthesis of a resorcinol formaldehyde (RF) gel followed by pyrolysis under an inert atmosphere. Surface oxidation can also be performed during the final stage of the pyrolysis by bleeding oxygen in the furnace, at the cost of reduced production yield. The non-oxidized NPS can collect up to 0.14 g g^{-1} of water at 90% relative pressure. Oxidized NPS demonstrated significant improvements with water uptake of 0.28 g g^{-1} at 90% relative pressure and 0.14 g g^{-1} at 40% relative pressure. Both of these can be cycled multiple times without performance degradation. In addition, their fast kinetics makes them competitive to metal-organic frameworks (MOF) when assessed on their daily water yield instead of water uptake only.[9] Daily water yield is a metric combining the water uptake performance of a sorbent and its kinetics to assess how much water can be produced in a single day through multiple sorption and desorption cycles.

RF gel was first synthesized by Pekala using sol-gel technology in 1989, based on the production of inorganic silica gels.[10] Three main steps are involved in the production of RF gels and contribute to the final structure and properties of the carbon gel:

1) Synthesis of the wet RF gel, that includes making the sol mixture followed by gelation and finally curing of the gel;
2) Drying the wet RF gel to form an aerogel or a xerogel;
3) Carbonization of the dried gel through pyrolysis under an inert atmosphere such as Ar and N_2, which can also include activation.

During synthesis, the ratio of resorcinol to formaldehyde, resorcinol to catalyst, and resorcinol to solvent (typically water or ethanol), as well as type of catalyst and initial pH of the solution are important parameters that control the final properties.[11,12] In addition, the mass ratio M, which refers to the proportion of the monomers' mass relative to the total weight of the initial solution, has a significant impact on the pore widths, pore volumes, and total surface areas of the produced samples. At increased solvent loading, the space among the sol particles grows. This makes the pores in the gel bigger and more numerous once the solvent is evaporated.[13] There is also a direct correlation between M and the homogeneity of the final product. When the M value is low, the RF gels produced are heterogeneous, but when the M value is high, the RF gels are homogeneous.[12]

Sodium carbonate is generally considered both as a catalyst and a pH control agent in RF gel synthesis.[12,13] During reaction, some sodium carbonate is left within the bulk of the RF gel, while the rest stays within the unreacted liquid fraction.

The drying process of RF gels can lead to the formation of an aerogel or a xerogel depending on the process employed. Previous researchers have explored both types of gel for various applications.[12] Generally, drying under ambient air leads to the formation of a xerogel due to significant shrinkage, while supercritical CO_2 drying forms an aerogel.

During gel pyrolysis, chemical bonds are broken down using heat. The volume of the micropores in RF gels rises during the process as a direct result from the shrinking of mesopores. The overall pore volume of the carbon gel, on the other hand, remains the same.[12,14] Similar to synthesis, various parameters affect the final properties of pyrolyzed samples. Pyrolysis temperature, time and heating rate are the most important parameters investigated by various researchers. Namely, it seems that a higher heating rate did not appreciably alter the structure of pores in the carbon xerogels.[15] When the pyrolysis temperature increases, the total number of pores remains unchanged, but there are more micropores because the mesopores shrink.[12]

With the appropriate activation method, different functional groups can be added to the surface of carbonized materials. Physical or chemical methods of activation can be used for this work. Physical activation involves exposing the previously carbonized sample to oxidants such as carbon dioxide, oxygen, and ozone at high temperature. The activation process involves the incorporation of oxygenated surface groups into the surface of the carbon.[16-18] Although carbonization and activation were used in consecutive steps in various prior research works, few articles investigated the combination of these two steps. Combining the pyrolysis and activation stages reduces the required time and energy for the production of activated carbons.[19] This work investigates the effect of combined carbonization/activation under CO_2 atmosphere and its effect on water uptake of the resulting NPS. Based on the information presently available, this approach will provide a stable water harvesting material with high water uptake and low production costs. The production of this material could be scaled up to meet the pressing need for alternative, sustainable drinking water sources.
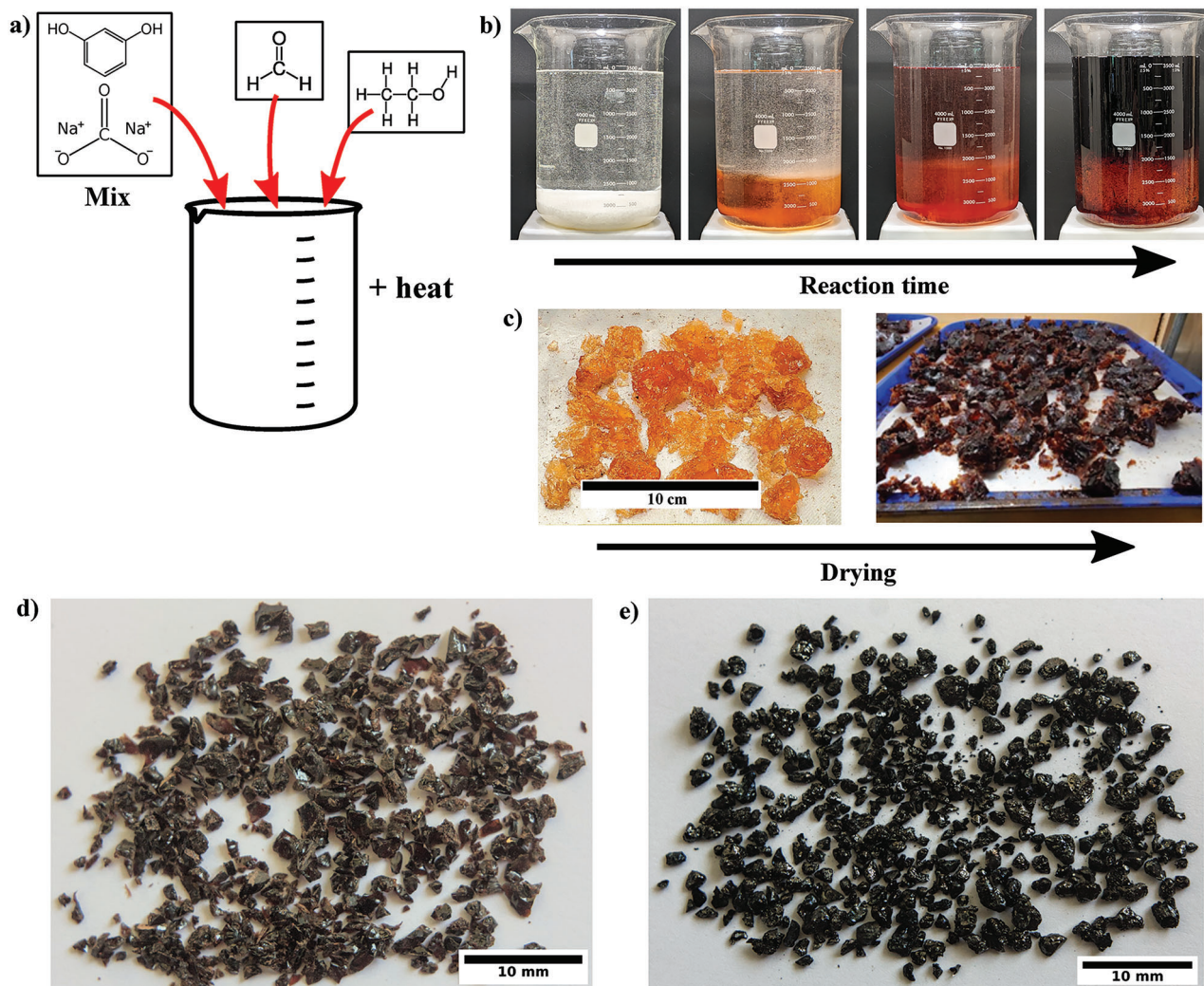
2. Methodology

2.1. Material

Resorcinol flakes FG (CAS 108-46-3) at >98% purity were purchased from Sigma-Aldrich. Anhydrous sodium carbonate certified ACS powder (CAS 497-19-8) with >99.5% purity and 37% wt formaldehyde (CAS 50-00-0) aqueous solution (F79P-4) were purchased from Fisher Chemical. Ethyl alcohol (95% vol) was purchased from Greenfield Global. CO_2 (99.8% pure) and argon (Ar) (99.999% pure) were purchased form Air Liquide.

2.2. Resin Synthesis

Batches of RF gel were synthesized in a 4 L beaker on a hot plate (**Figure 1**a) set at 120 °C. Resorcinol flakes were poured in the beaker followed by sodium carbonate. Both reagents were thoroughly mixed with a spatula. Formaldehyde was quickly poured to provide turbulent mixing and ethyl alcohol was added last. The solution was continuously heated without agitation for ≈2 h on the hot plate until the bottom half of the beaker formed a gel layer through which bubbles were unable to escape (Figure 1b).

The dark supernatant liquid on top of the gel (Figure 1b) was discarded in a separate container. The gel was cut into 2–3 cm pieces and completely dried in the fume hood at ambient conditions before further processing (Figure 1c). The dried gel was ground with a Paderno conical bur grinder Model No. CGR034 at its largest setting (Figure 1d). Subsequent grinding, with a smaller grinding setting, was also performed to produce batches of finer resin. Grinding of the resin is performed before pyrolysis to improve the mass transport of CO_2 to the surface of the RF gel. **Table 1** presents two formulations explored for this work.

2300309 (2 of 10)

**ADVANCED
SCIENCE NEWS**

www.advancedsciencenews.com

**ADVANCED
SUSTAINABLE
SYSTEMS**

www.advsustainsys.com

Figure 1. Production process of the NPS presenting a) order of reagents addition, b) evolution of the RF solution during synthesis c) RF gel evolution during the drying process d) dry RF resin after grinding and e) pyrolyzed NPS.

2.3. Pyrolysis

The pyrolysis experiments were performed in an MTI GSL-1500X-50 horizontal tube furnace using a quartz tube (O.D. 50.8 mm I.D. 47.6 mm). The resin was evenly distributed as a thin layer, no more than 3 mm thick, in a ceramic crucible and then inserted at the center of the furnace before pyrolysis.
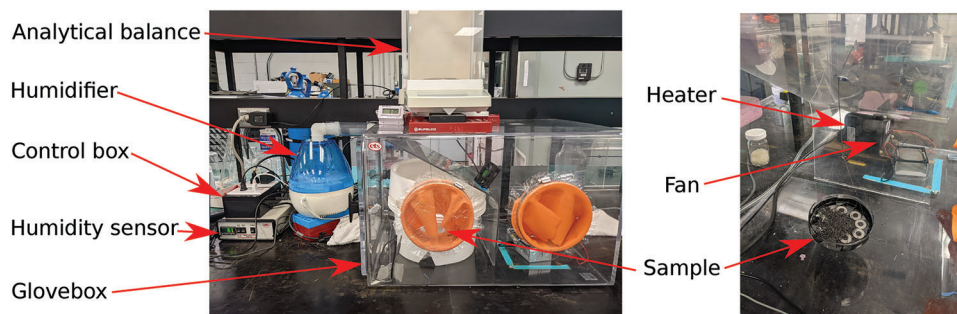
Table 1. Gel formulations.

Reagent	Weight %	
	Formulation A	Formulation B
Resorcinol	18	25
Sodium carbonate	0.5	0.6
Formaldehyde	27	38
Ethyl alcohol	55	36

The gas flow at the inlet of the furnace was controlled with a Tylan FC-260 mass flow controller. The outlet was connected to ventilation. The furnace was heated at a rate of 12°C min⁻¹ up to 820 °C. CO_2 was introduced from the beginning of the process. Three different flowrates of CO_2 were tested: 170 SCCM, 360 SCCM and 720 SCCM. After 3 h at 820 °C, the furnace's heating system was turned off and allowed to cool naturally. Meanwhile, CO_2 flow was discontinued, and the line was left to drain while Ar was added in the reactor at a flow rate of 360 SCCM. The RF gel is transformed into NPS during the pyrolysis (Figure 1e).
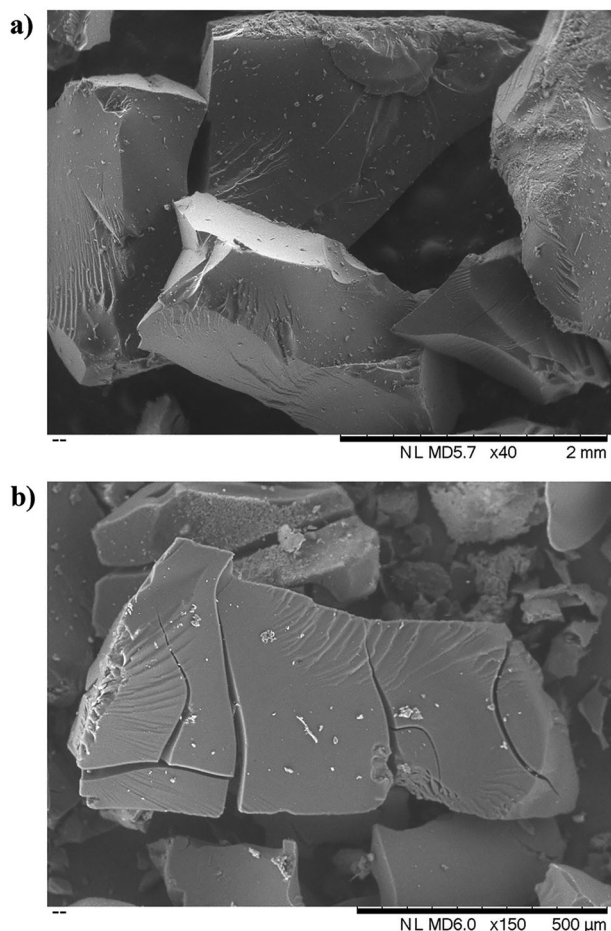
2.4. Characterization

2.4.1. Dynamic Vapor Sorption

Sorption measurements were performed with a custom-built, computer-controlled dynamic vapour sorption system (DVS). The system consists of a glovebox coupled with an analytical

ADVANCED
SCIENCE NEWS
www.advancedsciencenews.com

ADVANCED
SUSTAINABLE
SYSTEMS
www.advsustainsys.com

Figure 2. Custom-built dynamic vapor sorption system.

Figure 3. SEM images from a) RF resin before pyrolysis and b) NPS after pyrolysis.

balance, a humidity sensor, a temperature sensor, a humidifier, a source of dry air, a fan and a heater (**Figure 2**), controlled from a LabView interface.

A complete DVS analysis is performed by subjecting a sample of ≈500 mg of dried NPS to a cyclic relative pressure fluctuation from 5% to 95% and back to 5%, in 5% increments. The relative pressure condition is changed only when the weight of the sample has completely stabilized. The temperature in the system is kept constant at 30 °C.

During analysis, the weight of the sample is recorded every 5 s. The water uptake, described in Equation 1, is estimated for each relative pressure condition by calculating the average of the last 5 min of each step.

$$Water\ uptake\ (g/g) = \frac{(Mass\ of\ sample - Dry\ mass\ of\ NPS)}{Dry\ mass\ of\ NPS} \quad (1)$$

In addition to complete DVS analysis, which requires a significant amount of time, exploratory experiments were performed. In this "fast DVS" test procedure, a dry sample is installed in a 95% relative pressure atmosphere and the water uptake over time is monitored. Daily water yield can be estimated from the sorption kinetics of the sorbent.[9]

Finally, robustness experiments were performed by repeatedly cycling the relative pressure in the atmosphere around the sample between 5% and 95% while monitoring water uptake.

2.4.2. Gas Physisorption

Gas physisorption measurements were performed with a Micromeritics Gemini VII under N_2 to calculate the BET (Brunauer, Emmett and Teller) specific surface area, the total micropores volume and their size distribution. Samples were degassed before the tests at 300 °C over 12 h and their final weight was between 0.15 g and 0.20 g. Non-local density functional theory (NLDFT) was used to characterize the micropore size distribution of the samples. A NPS sample pyrolyzed under an Ar atmosphere served as a reference.

2.4.3. X-ray Photoelectron Spectroscopy

The surface composition of pyrolyzed NPS were characterized by X-ray photoelectron spectroscopy (XPS) with a Thermo Scientific K-Alpha. The X-ray source was an aluminum-kα with a spot size of 400 µm. Survey scans were performed with a pass energy of 200 eV and step size of 1 eV. High-resolution spectra of O1s and C1s peaks were performed with a pass energy of 50 eV and step size of 0.1 eV. Binding energies were compared to references from the literature.[20]

Table 2. Effect of pyrolysis on particle size distribution of RF resin at the largest grind setting.

		Ground RF resin	NPS
Dx10	[μm]	561	551
Dx50	[μm]	1239	1075
Dx90	[μm]	2173	1946
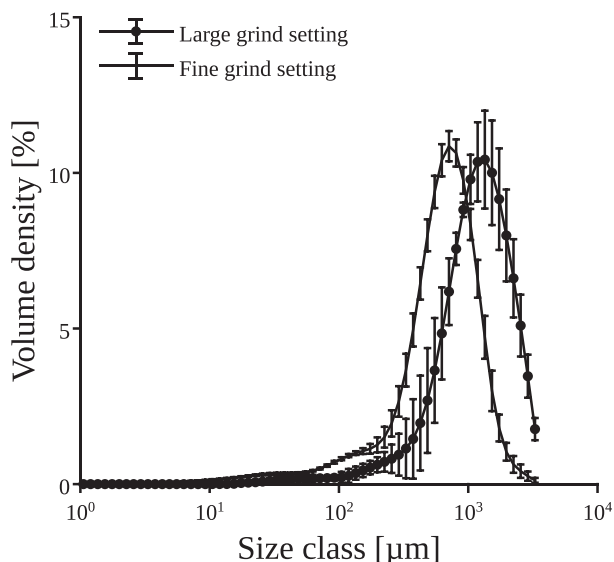
Figure 4. Particle size distribution for ground RF resin before pyrolysis.

2.4.4. Bulk Density

Samples of NPS were poured into a graduated cylinder until they occupied a volume ranging from 5 to 10 mL. The final mass and volume of the samples were then used in Equation 2 to evaluate the bulk density:

$$bulk\ density = \frac{mass\ of\ NPS}{volume\ occupied\ by\ NPS} \tag{2}$$

2.4.5. Particle Size

Size distribution of NPS before and after pyrolysis were measured with a Mastersizer 3000 from Malvern Panalytical with a hydro cell. The particles were dispersed in water for the test.

Table 3. Results from the BET analysis for NPS from formulation A pyrolyzed under Ar or CO2 atmospheres and NPS from formulation B pyrolyzed under CO2 atmosphere.

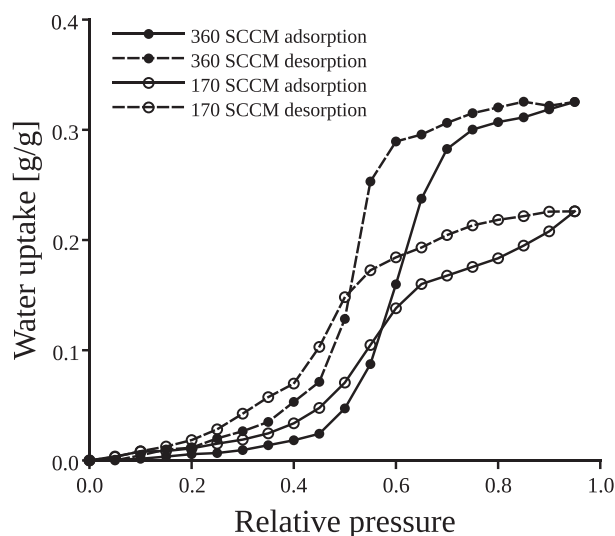|		NPS [A]	NPS CO_2 [A]	NPS CO_2 [B]
BET surface area	[m² g⁻¹]	509	1301	884
T-plot micropore volume	[cm³ g⁻¹]	0.224	0.480	0.328
T-plot micropore area	[m² g⁻¹]	446	956	654
T-plot external surface area	[m² g⁻¹]	63	345	230
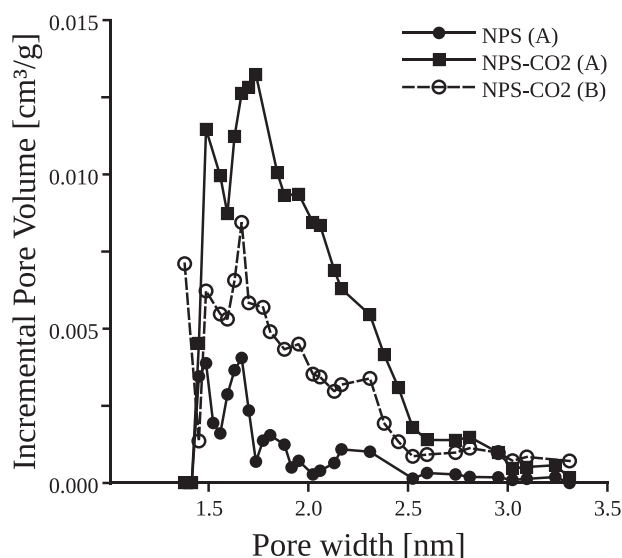
Figure 5. Incremental pore volume distribution by pore width from NLDFT analysis for NPS from formulation A pyrolyzed under Ar (NPS A) or CO_2 atmospheres (NPS CO2 A) and NPS from formulation B pyrolyzed under CO_2 atmosphere (NPS CO2 B).
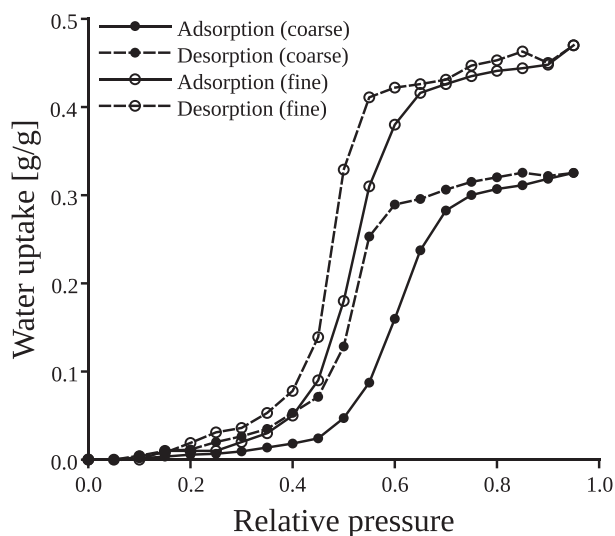
2.4.6. Morphology Analysis

The morphology of the resin before and after pyrolysis was imaged with a Hitachi TM3030 plus tabletop scanning electron microscope.

3. Results and Analysis

After pyrolysis, the NPS particles have a dark shiny surface (Figure 1e). The yield of NPS after pyrolysis was between 25% and 35%. The resulting particles had a bulk density of 0.40 g cm⁻³ for formulation A and 0.28 g cm⁻³ for formulation B.
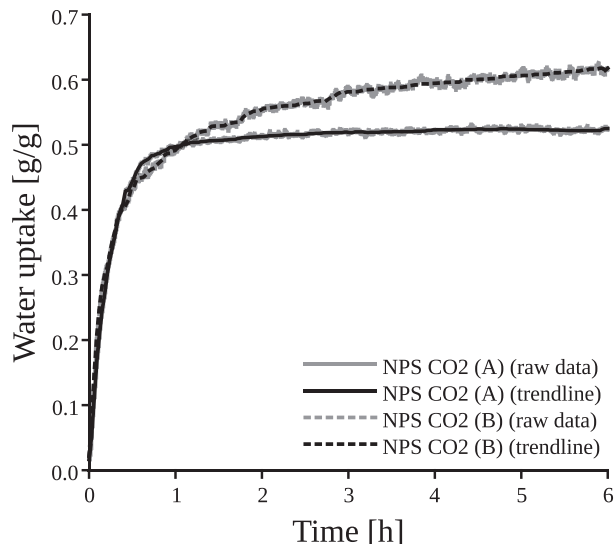

Figure 6. Effect of CO_2 flow rate on the water uptake for formulation A.

**ADVANCED
SCIENCE NEWS**

www.advancedsciencenews.com

**ADVANCED
SUSTAINABLE
SYSTEMS**

www.advsustainsys.com

Figure 7. Effect of grinding size before pyrolysis on the water uptake for formulation A.

Figure 9. Fast DVS comparing initial water uptake over time for formulations A and B at a constant relative pressure of 95%. Trend lines are superimposed in black over the raw data in grey to highlight the rate of water uptake over 6 hours.

Before pyrolysis, the resin exhibit smooth and angular surfaces with minor signs of fracture propagation from the volumetric shrinking during the drying process and the following grinding process (**Figure 3**a). After pyrolysis, the structure is opened-up with slit fractures through the bulk of the NPS (Figure 3b).
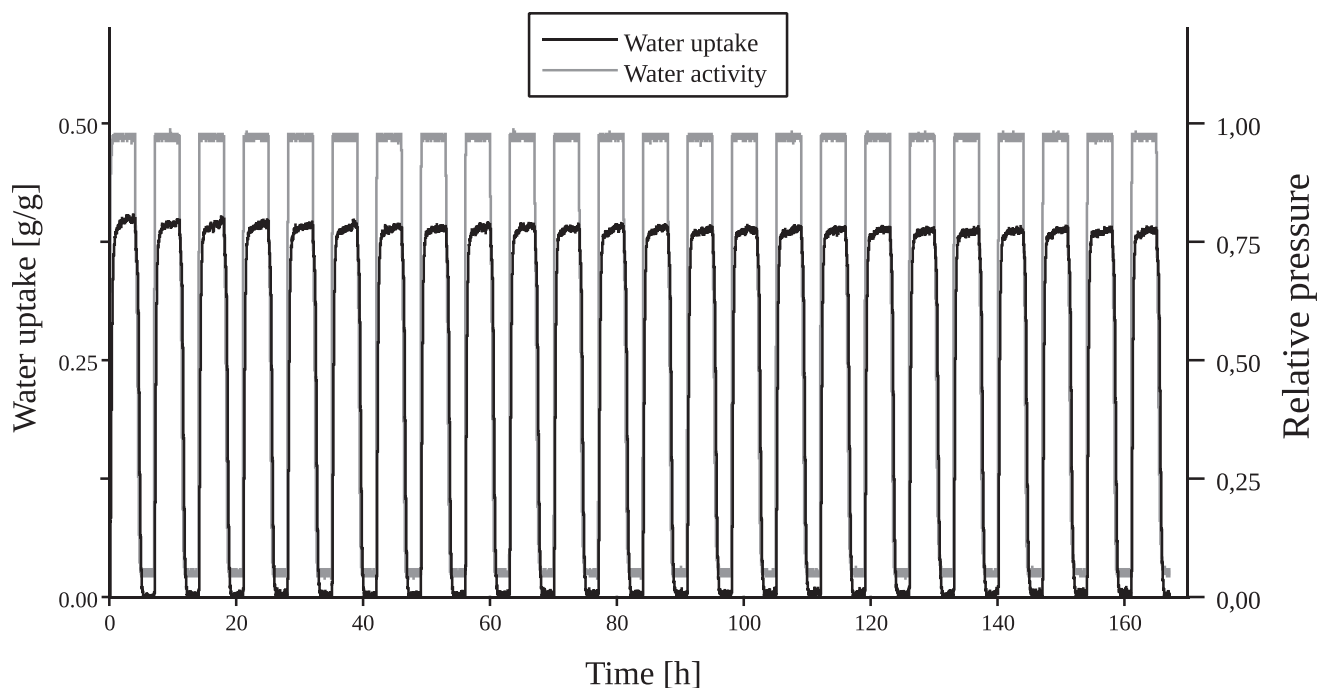
During pyrolysis, CO_2 acts as an oxidizer similar to oxygen used in previously published results.[8] At high flow rate (720 SCCM), the sample was completely consumed during the pyrolysis process. Further characterization was only performed

on samples using the low (170 SCCM) and normal (360 SCCM) flow rate.

The particle size distribution of dried RF resin ground at the largest setting and the resulting NPS particle after pyrolysis are presented in **Table 2**. The particles ground at the largest setting are mostly millimeter-sized with a narrow distribution as presented in **Figure 4**. Secondary grinding produced a similar but smaller particle size distribution. Pyrolysis caused an

Figure 8. Repeated DVS cycles for NPS CO_2 from formulation A.

**ADVANCED
SCIENCE NEWS**

www.advancedsciencenews.com

**ADVANCED
SUSTAINABLE
SYSTEMS**

www.advsustainsys.com

approximately 13% shrinkage to the average particle size of the large particles.

Calculation of BET specific surfaces and NLDFT analyses for NPS from formulation A pyrolyzed under Ar or CO_2 atmospheres and NPS from formulation B pyrolyzed under CO_2 atmosphere are presented in **Table 3** and in **Figure 5**. Pyrolysis of formulation B under an Ar atmosphere was not performed. CO_2 pyrolysis increased the surface area available and the total volume of the micropores. NLDFT analysis also confirmed that a significant fraction of pores have diameters below the critical pore size required for water nucleation by capillary condensation to minimize hysteresis (2.2 nm at 298 K). NPS synthesized under CO_2 using formulation A show an increased amount of porosity below this critical threshold, which correlates with increased water uptake.

Pyrolysis under Ar or CO_2 opens up a network of narrow slits and pores within the structure of the resin. The microporous structures present between the clusters formed during the gel synthesis[21] connect during pyrolysis to form a continuous open network. The CO_2 atmosphere a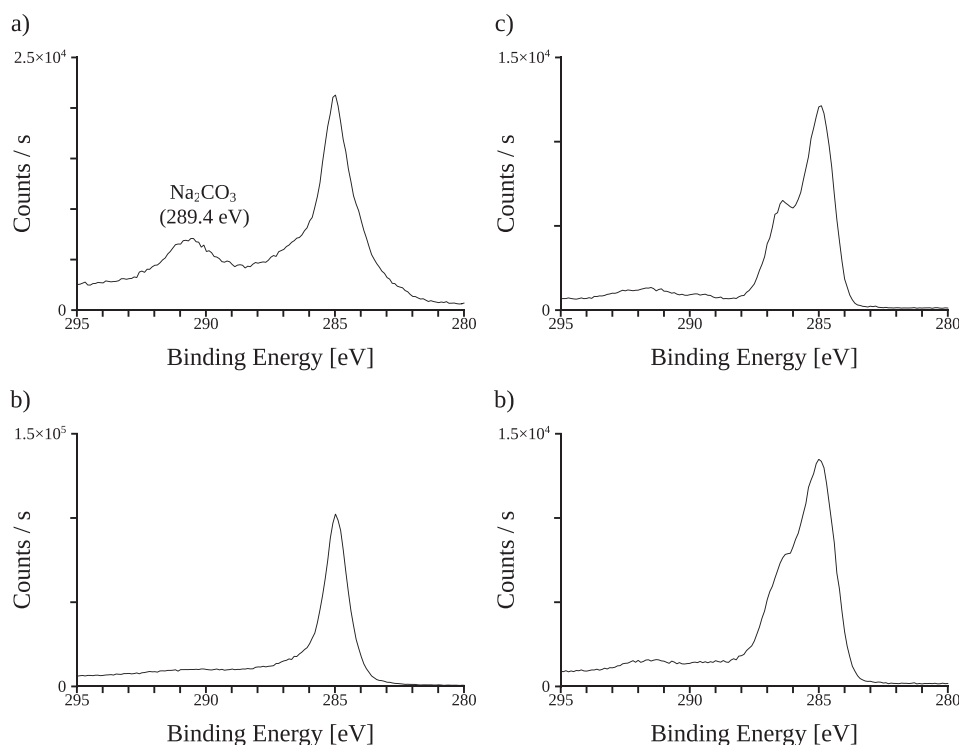dds a slightly oxidizing effect similar to the introduction of air,[8] but with reduced and thus more controlled kinetics.

The flow rate of CO_2 during pyrolysis has a significant effect on the water uptake performance of the resulting NPS. **Figure 6** compares the water uptake for different relative pressure conditions in samples pyrolyzed under normal and reduced CO_2 flow rate. Insufficient CO_2 flow hinders the activation process. The resulting NPS present significantly impaired water sorption at relative pressure and increased hysteresis. On the other hand, higher CO_2 flow (720 sccm) totally consumes the NPS during the pyrolysis process. A balance must be maintained between the water uptake performance of the NPS and economic viability.

As shown in **Figure 7**, the particle size before pyrolysis is also a significant factor for the water uptake performance of NPS. Smaller particles led to increased surface area and larger connected pores total volume after the pyrolysis process. These physical improvements resulted in increased water uptake and reduced hysteresis. We can infer from that result that control over the mass transport of CO_2 during the pyrolysis process is a key aspect.
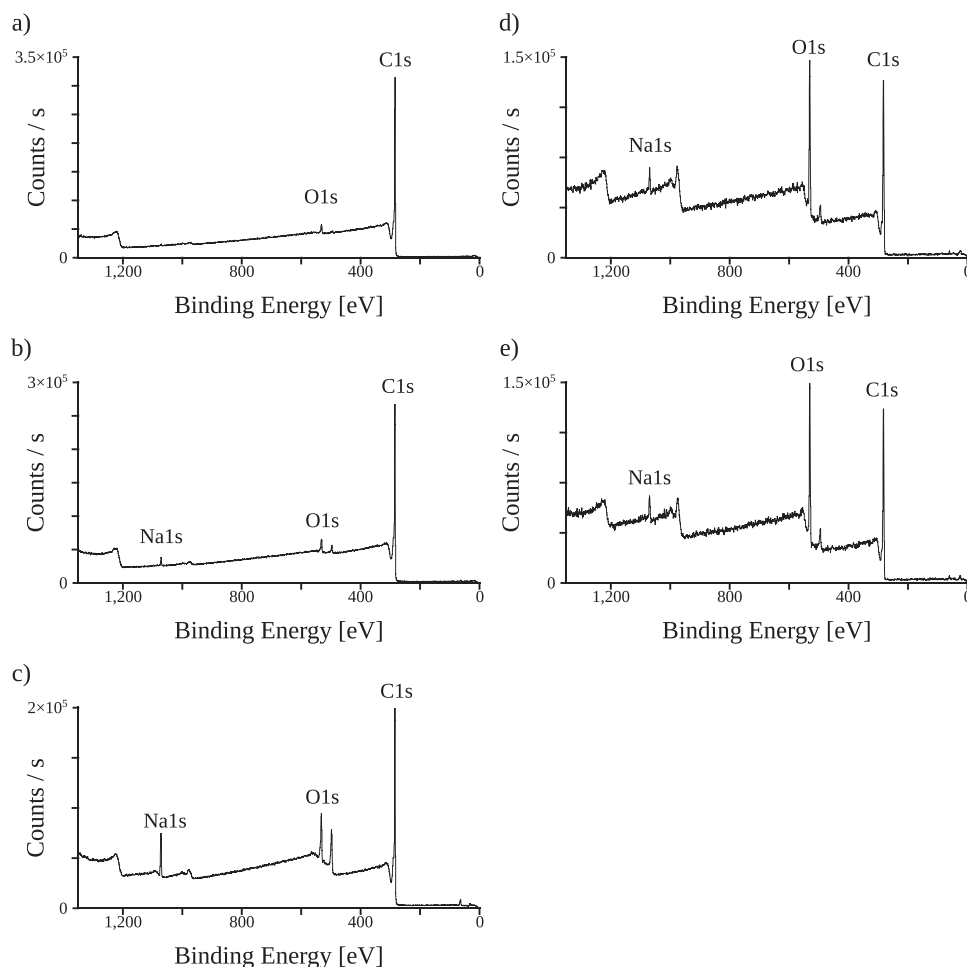
Figure 10. XPS survey scan for a) NPS (A) pyrolyzed under Ar, b) NPS CO_2 (A), c) NPS CO_2 (B) both pyrolyzed under 360 SCCM of CO_2 presenting increasing concentration of sodium, d) RF resin from formulation A and e) RF resin from formulation B.
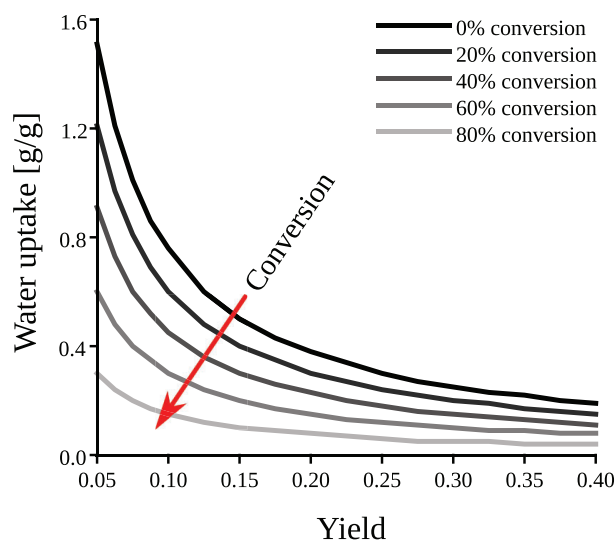
2300309 (7 of 10)

ADVANCED
SCIENCE NEWS
www.advancedsciencenews.com

ADVANCED
SUSTAINABLE
SYSTEMS
www.advsustainsys.com

Figure 11. High resolution XPS scan of the C1s peak showing Na_2CO_3 peak at 289.4 eV[20] for a) NPS CO_2 (B), b) NPS CO_2 (A) samples, c) RF resin from formulation A and d) RF resin from formulation B.

In addition to high water uptake, a sorbent for AWH needs to maintain good performance over a large number of cycles to be commercially viable. **Figure 8** presents the results of an endurance test with the NPS being subjected to cyclic humidity conditions, alternating between 5% and 95% water activity. Following an initial 2.5% decrease of their maximum water uptake after four cycles, the NPS maintained stable performance for more than 20 cycles.

An unexpected result was obtained for samples from formulation B. While samples from formulation A, under constant humidity conditions, reached a steady and repeatable water uptake, the water uptake for samples from formulation B, under the same conditions, kept increasing steadily over extended periods of time and would not stabilize, as shown in **Figure 9**. In one case, a sample constantly kept at a relative pressure of 95% reached over 1.2 g g^{-1} after 48 h. Repeated testing on the same sample would not reproduce the same behavior and a lower water uptake would be obtained at each subsequent run. Rinsing the NPS before testing them negates this effect.

XPS survey scans (**Figure 10**) and high-resolution scans (**Figure 11**) were performed on NPS samples from formulation A pyrolyzed under Ar and 360 SCCM CO_2 atmospheres as well as on a NPS sample from formulation B, resin from formulation A and resin from formulation B. The initial structure of the RF resin contains a significant fraction of oxygen bound within the carbon structure (Figures 10d,e). The double peak present in the high-resolution spectra of the C1s peak for both RF gel samples (Figures 11c,d) is indicative of the presence of oxygen linked to

C1s carbons located at 286.5 eV. The main peak around 285 eV indicates a combination of both sp3 graphitic carbon and sp2 carbons, while the secondary peak around 286.5 eV can be either sp2 or sp3 carbons bound to oxygen or hydroxyl groups in the case of sp3 carbons.[22] The high resolution scans of pyrolyzed samples present only a single peak related to a combination of sp3 and/or sp2 carbons. The presence of a CO_2 atmosphere during pyrolysis slows down the sodium carbonate thermal decomposition process into sodium oxide[23] that occurs at high temperature under an inert atmosphere. This leads to an increased sodium carbonate residual content (Figure 10a,b) in NPS pyrolyzed under CO_2, when compared to NPS pyrolyzed under Ar. The high concentration of sodium carbonate left in the resin from formulation B contributes to a higher final sodium carbonate presence (Figure 10c). The increased presence of sodium carbonate in NPS from formulation B was also confirmed in high-resolution scans of the C1s peak (Figure 11) with a peak ≈289.4 eV.[20] The deliquescent nature of sodium carbonate[24,25] explains the time dependant water uptake behaviour of unrinsed samples from formulation B (Figure 9). In samples from formulation A, low sodium carbonate residual content leaves capillary condensation in the pore structure as the only mechanism for water collection, leading to a stable water uptake once saturation is reached (after a fast initial water uptake). More broadly, increased conversion of sodium carbonate into sodium oxide leads to a reduced contribution of deliquescence on total water uptake. For samples from formulation B, both the residual sodium carbonate and capillary condensation are acting in tandem. In those samples, the water uptake measurements initially present the fast-acting behavior of

**ADVANCED
SCIENCE NEWS**

www.advancedsciencenews.com

**ADVANCED
SUSTAINABLE
SYSTEMS**

www.advsustainsys.com

Figure 12. Effect of residual sodium carbonate on the water uptake caused by deliquescence. Increased conversion of sodium carbonate into sodium oxide reduce the effect of deliquescence.

capillary condensation followed by the slower deliquescent effect of sodium carbonate.

The maximum water uptake of sodium carbonate is reached in its decahydrate state and is at its lowest in its anhydrous state. From the assumptions that all of the initial sodium carbonate is contained in the resin at the end of the reaction and that the sodium carbonate is in its anhydrous state after pyrolysis, we can estimate the maximum deliquescent effect of sodium as function of pyrolysis yield and sodium carbonate conversion efficiency (**Figure 12**). The additional water uptake from residual sodium carbonate calculated from this analysis is consistent with the values observed in our experiments.

Table 4 presents a summary of the water uptake performance for all NPS from formulation A at key relative pressure conditions. Water uptake values for NPS from formulation B are not reported, as it was impossible to obtain stable and reproducible measurements over multiple experiments.

Based on our findings, NPS produced from formulation A can serve as a baseline for future optimization of the pyrolysis process. While NPS from formulation B exhibit an interesting time-

dependant behavior, it is expected that NPS with stable performance will perform better in a future prototype.

4. Conclusion

Combining the pyrolysis and activation of RF resin in a single step under a CO_2 atmosphere significantly improves the water harvesting capability of the resulting NPS. With improved control over the mass transport of CO_2 through flow rate and grinding size for the resin prior to pyrolysis, we were able to significantly improve the water uptake at 95% relative pressure from 0.14 g g^{-1}[8] up to 0.47 g g^{-1}. These NPS exhibit the same stable, repeatable and fast performance over repeated endurance cycles as the original NPS. Further tests are planned to evaluate the effect of different catalysts during the production of RF resin and the resulting water harvesting capabilities of the NPS. The process presented within this article is straightforward and can readily be scaled using industrially mature technologies to reach the production level required to address global water scarcity issues.

Conflict of Interest

The authors D. Brassard, W. Raphael, J. R. Tavares and R. Boudreault have filed a patent on the NPS sorbents, and thus acknowledge their personal financial interest in this research. R. Boudreault is the CEO of Awn Nanotech Inc. the industrial partner supporting this research. This potential conflict of interest has not led any of the co-authors to bias or otherwise modify any of the methods and/or results reported here.

Data Availability Statement

The data that support the findings of this study are openly available in Polytechnique Montréal Dataverse at https://doi.org/10.5683/SP3/P22FRH.

Table 4. Summary of the water uptake values for NPS (A) and NPS CO_2 (A) as function of relative pressure for the test conditions reported in this article.

	NPS [A]	NPS CO_2 [A] 170 SCCM Coarse	NPS CO_2 [A] 360 SCCM coarse	NPS CO_2 [A] 360 SCCM fine
Relative pressure [%]	Water uptake [g g^{-1}]			
95	0.14	0.22	0.33	0.47
60	0.11	0.14	0.16	0.38
30	0.02	0.02	0.01	0.02

[1] M. M. Mekonnen, A. Y. Hoekstra, *Sci. Adv.* **2016**, *2*, 7.

[2] Z. Karimidastenaei, T. Avellán, M. Sadegh, B. Kløve, A. T. Haghighi, *Sci. Total Environ.* **2022**, *827*, 154429.

[3] H. Jarimi, R. Powell, S. Riffat, *International Journal of Low-Carbon* **2020**, *2020*, 253.

[4] D. Nioras, K. Ellinas, V. Constantoudis, E. Gogolides, *ACS Applied Materials and Interfaces* **2021**, *13*, 48322.

[5] A. Grosman, C. Ortega, *Langmuir* **2008**, *24*, 3977.

[6] T. Horikawa, D. D. Do, D. Nicholson, *Adv. Colloid Interface Sci.* **2011**, *169*, 40.

[7] A. J. Rieth, S. Yang, E. N. Wang, M. Dinca, *ACS Cent. Sci.* **2017**, *3*, 668.

[8] U. Legrand, D. Klassen, S. Watson, A. Aufoujal, B. Nisol, R. Boudreault, K. E. Waters, J.-L. Meunier, P.-L. Girard-Lauriault, M. R. Wertheimer, J. R. Tavares, *Ind. Eng. Chem. Res.* **2021**, *60*, 12923.

[9] U. Legrand, P.-L. Girard-Lauriault, J.-L. Meunier, R. Boudreault, J. R. Tavares, *Langmuir* **2022**, *38*, 2651.

[10] R. W. Pekala, *J. Mater. Sci.* **1989**, *24*, 3221.

[11] A. Awadallah-F, A. M. Elkhatat, S. A. Al-Muhtaseb, *J. Mater. Sci.* **2011**, *46*, 7760.

[12] A. M. Elkhatat, S. A. Al-Muhtaseb, *Adv. Mater.* **2011**, *23*, 2887.

[13] S. A. Al-Muhtaseb, J. A. Ritter, *Adv. Mater.* **2003**, *15*, 101.

[14] K. M. Steel, W. J. Koros, *Carbon N Y* **2005**, *43*, 1843.

[15] A. H. Moreno, A. Arenillas, E. G. Calvo, J. M. Bermúdez, J. A. Menéndez, *J. Anal. Appl. Pyrolysis* **2013**, *100*, 111.

[16] M. S. Contreras, C. A. Páez, L. Zubizarreta, A. Léonard, S. Blacher, C. G. Olivera-Fuentes, A. Arenillas, J.-P. Pirard, N. Job, *Carbon* **2010**, *48*, 3157.

[17] M. P. Chavhan, V. Slovak, G. Zelenkova, D. Dominko, *Materials* **2022**, *15*, 2431.

[18] M. A. Elsayed, P. J. Hall, M. J. Heslop, *Adsorption* **2007**, *13*, 299.

[19] A. Abolghasemi Mahani, S. Motahari, V. Nayyeri, *Mater. Chem. Phys.* **2018**, *213*, 492.

[20] J. F. Moulder, W. F. Stickle, W. M. Sobol, K. D. Bomben, Handbook of X-Ray Photoelectron Spectroscopy, **1992**.

[21] S. J. Taylor, M. D. Haw, J. Sefcik, A. J. Fletcher, *Langmuir* **2014**, *30*, 10231.

[22] B. Lesiak, L. Kövér, J. Tóth, J. Zemek, P. Jiricek, A. Kromka, N. Rangam, *Appl. Surf. Sci.* **2018**, *452*, 223.

[23] K. H. Stern, E. L. Weise, *Carbonates* **1969**.

[24] P. Yang, H. Yang, N. Wang, C. Du, S. Pang, Y. Zhang, *J. of Env. Sci.* **2020**, *87*, 250.

[25] O. F. Steinbach, *J. Chem. Educ.* **1943**, *20*, 146.